Available online at www.sciencedirect.com
ScienceDirect
International Journal of Thermal Sciences 47 (2008) 998–1011
International Journal of Thermal Sciences
www.elsevier.com/locate/ijts

Experimental and numerical investigation of convection heat transfer of CO_2 at supercritical pressures in a vertical tube at low Reynolds numbers

Pei-Xue Jiang *, Yu Zhang, Yi-Jun Xu, Run-Fu Shi

Key Laboratory for Thermal Science and Power Engineering of Ministry of Education, Department of Thermal Engineering, Tsinghua University, Beijing 100084, China

Received 13 May 2005; received in revised form 8 August 2007; accepted 8 August 2007

Available online 6 September 2007

Abstract

Convection heat transfer of supercritical pressure CO_2 in a vertical tube at low Reynolds numbers (less than 2500) was investigated experimentally and numerically. The tests investigated the effects of inlet temperature, pressure, mass flow rate, heat flux, buoyancy and flow direction on the heat transfer. For the lower heat flux of 4.49 kW/m^2, the numerical results corresponded well to the experimental data (within 8%). However, for heat fluxes higher than 13.7 kW/m^2, the numerical results for the convection heat transfer coefficient using laminar flow were much less than the experimental data over most of the tube (e.g., difference larger than 74% for $x/d = 15$) due to the strong influence of buoyancy and the decrease of the dynamic viscosity with temperature along the tube which results in an early transition from laminar to turbulent flow. The numerical results for the convection heat transfer coefficient using turbulent flow corresponded much better with the experimental data. The convection heat transfer coefficient increases with increasing heat flux and then decreases with further increases in the heat flux for both upward and downward flows. The flow direction significantly influences the heat transfer. For high heat flux (e.g., 61.0–94.0 kW/m^2) upward flow, the local wall temperature varies in a complex, nonlinear fashion, while for downward flow the local wall temperature increases monotonically and the heat transfer is strongly enhanced by buoyancy.

Keywords: Convection heat transfer; Supercritical pressures; Low Reynolds number; Buoyancy; Upward flow and downward flow

1. Introduction

Supercritical fluids (Water, CO_2, H_2, He, etc.) are widely used in various industries such as supercritical boilers in power engineering, supercritical CO_2 extraction and supercritical fluid chromatography in chemical engineering, rocket propulsion systems in aerospace engineering, cooling of superconducting electromagnets and superconducting electronics in cryogenics engineering, and more recently, transcritical CO_2 air-conditioning and heat pump systems in refrigeration engineering, and water oxidation systems for waste treatment. In the supercritical region, small fluid temperature and pressure variations lead to significant changes in the thermophysical properties as shown in Fig. 1. For a given supercritical pressure, the specific heat reaches a maximum at a specific temperature, which is called the pseudocritical temperature. Convection heat transfer of fluids at supercritical pressures has many special features due to these sharp variations of the thermophysical properties with temperature and pressure. The effect of buoyancy in the mixed convection regime can also be significant.

Internal forced and mixed convection heat transfer of supercritical fluids has investigated extensively in the past 50 years, especially in the 1950s–1980s with intensive investigations on this subject in the former USSR, the USA and the UK for developing supercritical boilers and Supercritical Pressure Water-cooled Reactors (SPWRs). Recently, there has been increasing interest in heat transfer of fluids at supercritical pressures in small/mini/micro scale tubes or channels and in porous media. This interest is driven by the need to develop the SPWR, nuclear reactors with supercritical CO_2 indirect cycles, mini or compact gas coolers and internal heat exchangers for the CO_2 high-pressure trans-critical compression cycle in air-conditioners and heat pumps, and by the need to improve transpiration

* Corresponding author.
E-mail address: jiangpx@tsinghua.edu.cn (P.-X. Jiang).

1290-0729/$ – see front matter
doi:10.1016/j.ijthermalsci.2007.08.003

Nomenclature

Bo^*	buoyancy number ($Gr^*/(Re^{3.425}Pr^{0.8})$)	
c_p	specific heat at constant pressure	J/(kg K)
c_p^+	dimensionless specific heat (C_p/C_{p_0})	
d	tube inner diameter	m
D	tube outer diameter	m
F_{in}	inner tube surface area	m^2
g	gravitational acceleration	m/s^2
G	mass flux	$kg/(m^2 s)$
Gr^*	Grashof number ($\beta g d^4 q_w/(\lambda\nu^2)$)	
h	specific enthalpy	J/kg
h^+	dimensionless specific enthalpy ($(h-h_0)/(q_w c_{p0} d/\lambda_0)$)	
$h_{f,0}$	specific enthalpy at inlet	J/kg
$h_{f,b}(x)$	local bulk fluid enthalpy	J/kg
h_x	local heat transfer coefficient	$W/(m^2\,°C)$
I	current through the heater and test section	A
L	test section length	m
L_t	total length in numerical simulation including unheated inlet and outlet sections	m
m	mass flow rate	kg/h
p	pressure	N/m^2
p^+	dimensionless pressure ($p^+ = p/(\rho_0 u_0^2)$)	
Pe	Peclet number ($Re\,Pr$)	
Pr	Prandtl number ($\mu c_p/\lambda$)	
q_v	volumetric heat flux ($4I^2R/(\pi(D^2-d^2)L)$)	W/m^3
q_w	heat flux on the inner tube surface	W/m^2
Q_{loss}	heat loss from the test section	W
r	radial coordinate	m
r^+	dimensionless radial coordinate (r/d)	
R	test section electrical resistance	Ω
Re	Reynolds number ($\rho u d/\mu = 4m/(\pi d\mu)$)	
T	temperature	°C or K
T_{pc}	pseudocritical temperature	°C or K
u	x direction component of velocity	m/s
u^+	x direction component of non-dimensional velocity (u/u_0)	
v	r direction component of velocity	m/s
v^+	r direction component of non-dimensional velocity (v/u_0)	
x	axial coordinate	m
x^+	dimensionless axial coordinate (x/d)	

Greek symbols

λ	thermal conductivity	W/(m K)
λ^+	dimensionless thermal conductivity (λ/λ_0)	
β	volume expansion coefficient	1/K
ρ	density	kg/m^3
ρ^+	dimensionless density (ρ/ρ_0)	
μ	dynamic viscosity	kg/(m s)
μ^+	dimensionless dynamic viscosity (μ/μ_0)	

Subscripts

b	bulk
c	numerical results
dw	downward flow
e	experimental data
f	fluid
i	inner surface
o	outer surface
s	solid wall
up	upward flow
w	wall
x	local values
0	tube inlet

Superscripts

+	dimensionless

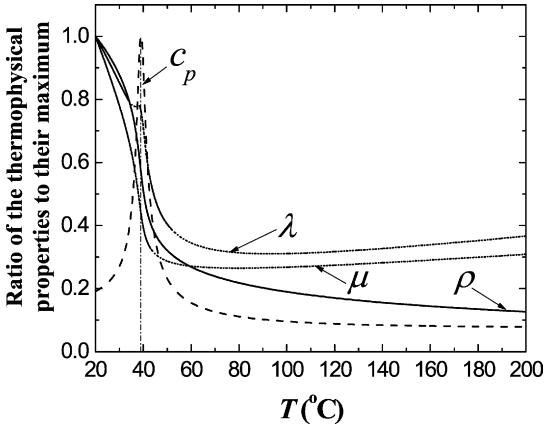

Fig. 1. Thermophysical properties of CO_2 at 8.85 MPa.

cooling of high temperature surfaces. As a result, significant progress has been achieved in our understanding of some of the special features and in correlating the experimental data for heat and mass transfer processes of supercritical pressure fluids [1–31]. A number of comprehensive reviews on convective heat transfer at supercritical pressures can be found in the literature, for example, Petukhov [1,2], Hall [3], Hall and Jackson [4], Polyakov [11], Jackson [16], Pioro et al. [22], Duffey and Pioro [27], and Pioro and Duffey [28].

These investigations [1–31] have shown that the sharp variations of the thermophysical properties with temperature and pressure at supercritical pressures significantly influence the heat transfer and flow resistance. The results show that there are three modes of heat transfer for fluids at supercritical pressures in vertical and horizontal tubes [1–5,7–14,16,21,22,24,26–30]: (1) normal heat transfer without deterioration at low heat fluxes and high mass fluxes, (2) deterioration of heat transfer with lower heat transfer coefficients (HTC) and higher temperatures over part of the heated section and (3) improved heat transfer with higher HTC. Fig. 1 shows how the specific heat varies with temperature and becomes very large in the vicinity of the pseud-

ocritical temperature. Therefore, for normal heat transfer at low heat fluxes and high mass fluxes, the HTC varies with temperature in relationship to the specific heat. The reduced heat transfer usually occurs at higher heat fluxes and lower mass fluxes due to acceleration and buoyancy near the wall due to the heating in upward flow in vertical tubes and in horizontal tubes. The reduced turbulence resulting from the flow acceleration due to the strong heating is one of the mechanisms causing the reduced heat transfer. Localized reduction of the heat transfer for upward flow in vertical tubes was explained in terms of partial laminarization of the flow due to strong buoyancy effects. However, the heat transfer is enhanced due to buoyancy for downward flow in vertical tubes and along the lower part of horizontal tubes.

In the past 50 years, there have been several hundred papers on heat transfer at supercritical pressures, with many heat transfer correlations. Pioro et al. [22,28] analyzed several typical correlations. Jackson [16] mentioned that a detailed evaluation of the many forced convection heat transfer correlations was carried out by their previous work. The various correlations were used to predict the HTC for approximately 2000 experimental conditions. The results showed that the 1965 approach of Krasnoshchekov and Protopopov [6] was easily the most effective. A particularly satisfactory aspect of its performance was that it was equally good for both water and carbon dioxide. Jackson et al. [9] gave a simpler form of that approach.

The influence of buoyancy on turbulence and heat transfer is a very important topic in research on heat transfer at supercritical pressures [1–5,7–14,16,20–22,24,26–30]. Bazargan et al. [24] mentioned that the effect of buoyancy was not properly addressed in some earlier studies, thus, many experimental results reporting forced convection heat transfer were really forced convection heat transfer with some buoyancy effects. The neglect of buoyancy is the primary reason for the considerable disagreement between predictions by the available empirical correlations. Therefore, the conditions for which buoyancy becomes important must be known. The experimental results in Bazargan et al. [24] showed that buoyancy effects are particularly important in horizontal flows, where flow asymmetry leads to a nonuniform local temperature distribution around the tube periphery. The criterion developed for buoyancy-free regions in near constant property flows is not adequate for predicting supercritical fluid flows. Numerical simulations by Kraan et al. [29] showed that for heated vertical flow of CO_2 without buoyancy, the variations of the thermophysical properties must be considered with the variable property relation of Krasnoshchekov and Protopopov [6] acceptable for design purposes. The criterion developed by Jackson and Hall [9,16] to determine when buoyancy is important was confirmed by CFD predictions. In the mixed convection regime for downward heated flow, CFD simulations gave results that agreed with the Jackson and Hall [9,16] buoyancy correction factor combined with the Krasnoshchekov–Protopopov relation [6].

In the past 50 years, theoretical analyses and numerical calculations have been applied to the heat transfer of fluids at supercritical pressures [1–4,10,11,16,21,23,26,29,30]. These calculations used modifications of the turbulence models based on mixing length theory [10,11] and two-equation models such as the k–ε model [21,23,26,29]. Direct numerical simulations of turbulent supercritical flows with heat transfer were performed by Bae et al. [30]. Their numerical results showed that simulations using proper turbulence models are able to reproduce the general features exhibited in experiments for convection heat transfer of fluids at supercritical pressures in vertical tubes. However, in other cases, the simulation results can be very different from the experimental data.

Although in the past 50 years extensive research has been done on convection heat transfer of supercritical fluids in tubes, to the authors' knowledge, there is very limited work on convection heat transfer of supercritical fluids at low Reynolds numbers (less than 2500) where the variation of the fluid properties and buoyancy can significantly affect the flow and convection heat transfer behavior. Polyakov [11] studied the influence of variable thermophysical properties and buoyancy on laminar heat transfer, but the transition from laminar to turbulent flow due to buoyancy was not investigated. In addition, there is little experimental data available for local convection heat transfer coefficients of supercritical pressure CO_2 in tubes with diameters less than 2.0 mm.

This paper describes experimental and numerical investigations of the convection heat transfer of supercritical pressure CO_2 in a 2.0 mm diameter vertical tube at low Reynolds numbers (less than 2500). The tests investigated the effects of inlet temperature and pressure, mass flow rate, heat flux, buoyancy and flow direction on the convection heat transfer. The transition from laminar to turbulence flow due to buoyancy was also investigated. The investigation of mixed convection heat transfer of a supercritical pressure fluid at low *Re* will lead to improved understanding of the heat transfer mechanisms. In addition, since the Reynolds numbers may be quite small in mini/micro tubes and channels in practice, this investigation of mixed convection heat transfer of supercritical pressure fluids at low *Re* also has important practical significance.

2. Experimental system and data reduction

2.1. Experimental system and parameter measurements

The experimental system and test section are shown schematically in Fig. 2. The system included a compressed CO_2 container, a supercritical CO_2 pump (Thar P-50, Thar Technologies, Inc., nominal flow rate is 0.06–3 kg/h, maximum discharge pressure is 689 bar and the inlet pressure for CO_2 is 57 bar), a cooling water bath and portable chiller, a CO_2 accumulator, a Coriolis mass flow meter, a pre-heater, a test section, a decompression valve, a pressure stabilizer, an aftercooler, pressure gauges, a total pressure transducer and a differential pressure transducer, electrical power input and measurement systems, and a data acquisition system (DAS).

The test section was a vertical stainless steel 1Cr18N9T tube with inside and outside diameters of 2 mm and 3.14 mm. The heated length of the test section was 39 mm. The test section was connected with the test loop by flanges and high-pressure fittings. The test sections were insulated thermally and electri-

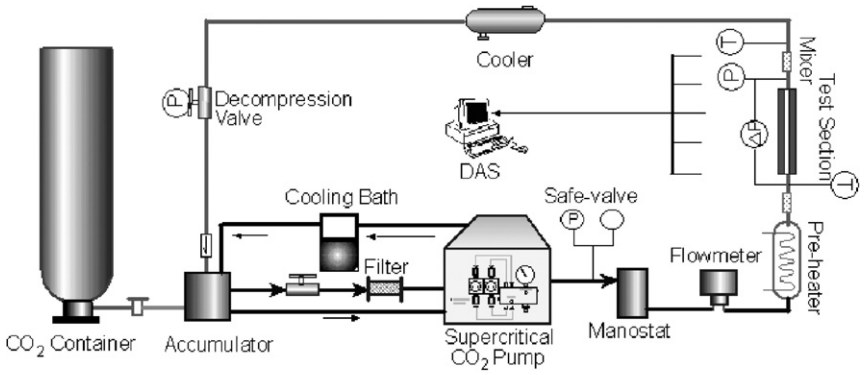

(a) Experimental system

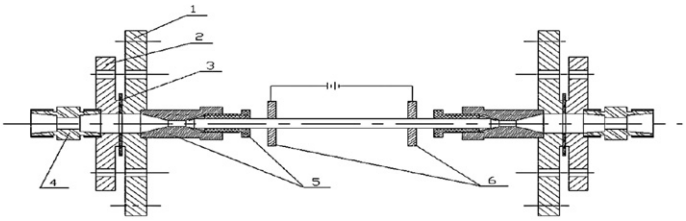

(b) Test section geometry

1—square flange 2—circular flange
3—polytetrafluoroethylene spacer (PTFE),
4, 5—connecting fittings 6—copper electrode

Fig. 2. Experimental system and test section.

cally from the test loop using a layer of polytetrafluoroethylene (PTFE) placed between the flanges and between the screws and the flanges. CO_2 flowed into the test section either from the bottom for upward flow or from the top for downward flow.

The test section was heated directly using low-voltage alternating current to simulate a constant heat flux. The voltages across the test section and the electrical heater were measured by the DAS. The current was measured by a digital multimeter (Model DM-7510B). The electric power inputs to the test section and the heater were calculated from the measured current, voltage and electrical resistance.

The parameters measured in the experiments included the wall temperatures, the inlet and outlet temperatures, the inlet pressure, the pressure drop across the test section, the mass flow rate, the heater voltages, the current and the electrical resistance. The local test section wall temperature was measured with 9 fine K-type thermocouples. The thermocouples were welded onto the tube outer surface. Flow mixers were installed upstream and downstream of the test section to mix the fluid before the inlet and outlet fluid temperatures were measured by accurate RTDs. The inlet pressure was measured using a pressure gage transducer (Model EJA430A) with the full range of 12 MPa. The test section pressure drop was measured using a differential pressure transducer (Model EJA110A) with the full range of 10 kPa. The mass flow rate was measured using a Coriolis-type mass flow meter (Model MASS2100/MASS6000, MASSFLO, Danfoss) with the full range of 65 kg/h.

Before the experiments, the test loop was evacuated with a vacuum pump. Then, the test loop was washed and evacuated 3–4 times using high purity CO_2 (99.995%). High pressure CO_2 with a purity of 99.995% was then fed into the test loop from the compressed CO_2 container to a steady pressure (about 5 MPa). The test loop pressure was increased using the high pressure CO_2 pump to the required supercritical pressure as the CO_2 was circulated. Many tests showed that the leakage was very small even for very high pressures (e.g. 10 MPa). The test section and most of the test loop were insulated with silicate glass fiber and foam pipe insulation.

2.2. Data reduction

The wall of the tube with inside and outside diameters of 2 mm and 3.14 mm was quite thin; therefore, the heat transfer in the tube was assumed to be one-dimensional heat conduction with an internal heat source when the tube was heated directly using the low-voltage alternating current. The outer surface was insulated and the tube outer surface temperatures, $T_{w,o}(x)$, were measured by the thermocouples. The tube inner surface temperatures, $T_{w,i}(x)$, were then calculated as

$$T_{w,i}(x) = T_{w,o}(x) + \frac{q_v}{16\lambda_s}\left(D^2 - d^2\right) + \frac{q_v}{8\lambda_s} D^2 \ln\frac{d}{D} \tag{1}$$

The local HTC, h_x, at each axial location was calculated as

$$h_x = \frac{q_w}{T_{w,i}(x) - T_{f,b}(x)} \tag{2}$$

The heat flux on the inner surface, q_w, was calculated using

$$q_w = \frac{I^2 R - Q_{\text{loss}}}{F_{\text{in}}} \tag{3}$$

Although the outer surface of the test section was insulated by glass fiber insulation and foam pipe insulation, the surface can not be assumed to be perfectly insulated. Before the experiments, the heat losses from the test section without fluid flow (Q_{loss}) were determined by measuring the electrical heating for different wall temperatures. Q_{loss} was found to be less than 5.8% of the electrical heating to the test section. In the data reduction, Q_{loss} was calculated based on the measured wall temperature and then subtracted from the total heat inputs, Eq. (3).

The local bulk fluid temperature, $T_{f,b}(x)$, was calculated from the local bulk fluid enthalpy, $h_{f,b}(x)$, which was in turn calculated from

$$h_{f,b}(x) = h_{f,0} + \frac{q_w \pi d x}{m} \tag{4}$$

The Reynolds number based on the mean fluid temperature was defined as

$$Re = \frac{\rho u d}{\mu} = \frac{4m}{\pi d \mu} \tag{5}$$

The system was determined to be at steady state when the variations of the wall temperatures and the inlet and outlet fluid temperatures were all within ±0.1 °C and the variations of the flow rate and inlet pressure were all within ±0.2% for at least 10 min. The experimental uncertainty of the HTC was mainly caused by experimental errors in the heat balance, axial thermal conduction in the test section, temperature measurement errors and the calculation of the heat transfer surface temperature.

Prior to installation, the thermocouples and the RTDs were calibrated by the National Institute of Metrology P.R. China. The accuracies were within ±0.1 °C in the temperature range of 0–100 °C and ±0.2 °C in the temperature range of 100–200 °C. The accuracy of the pressure transducer (Model EJA430A) was 0.075% of the full range of 12 MPa. The accuracy of the differential pressure transducer (Model EJA110A) was 0.075% of the full range of 10 kPa. According to the instructions, the accuracy of the Coriolis-type mass flow meter (Model MASS2100/MASS6000, MASSFLO, Danfoss) was 0.1% of actual mass flow rate with 95% confidence (probability) for flow with 5–100% of the sensor's maximum flow rate. For flow <5% of the sensor's maximum flow rate, the following formula should be used to calculate the error:

$$\varepsilon_G = \pm\sqrt{0.1^2 + \left(\frac{Z \times 100}{m}\right)^2}$$

Where ε_G = Error (%), Z = Zero point error (kg/h) (= 0.002 kg/h), and m = Mass flow (kg/h). The flow rate during the measurements was about 0.7 kg/h. Therefore, the relative uncertainty of the mass flow rate was 0.30%.

A detailed analysis of the uncertainty based on the instrument accuracies yielded a maximum uncertainty of the heating into the test section of ±8.3%, an uncertainty of the local bulk fluid temperature of ±0.2 °C and a relative uncertainty of the temperature drop between the wall and fluid of ±5.7%. The experimental uncertainties in the inlet pressures were estimated to be ±0.13%. The root-mean-square experimental uncertainty of the HTC was estimated to be ±10.1%.

3. Physical and mathematical models for upward laminar flow

The physical model and coordinate system are shown in Fig. 3. The model considers convection heat transfer to CO_2 at supercritical pressures in upward flow in a vertical tube. The test section consisted of an adiabatic section and a heated section with a constant heat flux. Flow enters the tube with a fully-developed velocity distribution and constant temperature, T_0. The flow is assumed to be two-dimensional, steady, laminar flow. The longitudinal conduction in the fluid and the pressure variation in the r direction are assumed to be negligibly small.

The steady state, two-dimensional laminar boundary layer governing equations for supercritical pressure fluid flow in a vertical tube with consideration of property variations with temperature and pressure and with buoyancy can be written as:

Equation of continuity:

$$\frac{\partial(r\rho u)}{\partial x} + \frac{\partial(r\rho v)}{\partial r} = 0 \tag{6}$$

Momentum equation for compressible fluids:

$$\rho u \frac{\partial u}{\partial x} + \rho v \frac{\partial u}{\partial r} = \frac{1}{r}\frac{\partial}{\partial r}\left(r\mu \frac{\partial u}{\partial r}\right) - \rho g - \frac{\mathrm{d}p}{\mathrm{d}x} \tag{7}$$

Energy equation:

$$\rho u \frac{\partial h}{\partial x} + \rho v \frac{\partial h}{\partial r} = \frac{1}{r}\frac{\partial}{\partial r}\left(r \frac{\lambda}{c_p}\frac{\partial h}{\partial r}\right) + u\frac{\mathrm{d}p}{\mathrm{d}x} + \mu\left(\frac{\partial u}{\partial r}\right)^2 \tag{8}$$

Flow rate equation:

$$\frac{\pi d^2}{4}\rho_0 u_0 = \int_0^{d/2} 2\pi r \rho u \,\mathrm{d}r \tag{9}$$

The boundary conditions are that the inlet conditions are a fully developed velocity profile and constant fluid temperature (Eq. (10)), symmetry at the centerline (Eq. (11)), and the

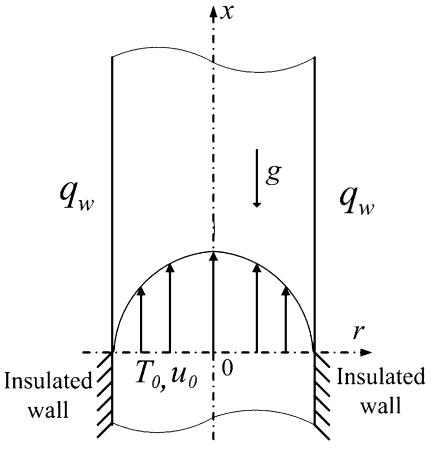

Fig. 3. Physical model.

no slip and constant heat flux boundary conditions at the wall (Eq. (12)).

$$x=0,\quad \frac{u}{u_0}=2\left[1-\left(\frac{2r}{d}\right)^2\right],\ v=0,\ T=T_0 \tag{10}$$

$$x>0,\quad r=0,\ \frac{\partial u}{\partial r}=\frac{\partial h}{\partial r}=0,\ v=0 \tag{11}$$

$$r=d/2,\ u=0,\ v=0,\ \left(\frac{\lambda}{c_p}\frac{\partial h}{\partial r}\right)_w=q_w \tag{12}$$

The dimensionless form of the governing equations (Eqs. (6)–(9)), was based on the following dimensionless variables:

$$x^+=x/d,\quad r^+=r/d,\quad u^+=u/u_0,\quad v^+=v/u_0,$$
$$u_0=\overline{\rho u}/\rho_0,\quad p^+=p/(\rho_0 u_0^2),\quad h^+=(h-h_0)/(q_w c_{p0} d/\lambda_0)$$
$$\rho^+=\rho/\rho_0,\quad \mu^+=\mu/\mu_0,\quad \lambda^+=\lambda/\lambda_0,\quad c_p^+=c_p/c_{p0}$$

The dimensionless governing equations are then:

$$\frac{\partial(r^+\rho^+u^+)}{\partial x^+}+\frac{\partial(r^+\rho^+v^+)}{\partial r^+}=0 \tag{13}$$

$$\frac{\partial(\rho^+u^+u^+)}{\partial x^+}+\frac{\partial(\rho^+v^+u^+)}{\partial r^+}=\frac{1}{r^+}\frac{\partial}{\partial r^+}\left(r^+\frac{\mu^+}{Re_0}\frac{\partial u^+}{\partial r^+}\right)-\frac{d}{u_0^2}g\rho^+-\frac{\mathrm{d}p^+}{\mathrm{d}x^+} \tag{14}$$

$$\frac{\partial(\rho^+u^+h^+)}{\partial x^+}+\frac{\partial(\rho^+v^+h^+)}{\partial r^+}=\frac{1}{r^+}\frac{\partial}{\partial r^+}\left(r^+\frac{\lambda^+}{c_p^+}\frac{1}{Re_0Pr_0}\frac{\partial h^+}{\partial r^+}\right)+\frac{u_0^2}{q_w c_{p0} d/\lambda_0}u^+\frac{\mathrm{d}p^+}{\mathrm{d}x^+}+\frac{\mu_0u_0\lambda_0}{q_w c_{p0}\rho_0 d^2}\mu^+\left(\frac{\partial u^+}{\partial r^+}\right)^2 \tag{15}$$

$$8\int_0^{0.5}\rho^+u^+r^+\,\mathrm{d}r=1 \tag{16}$$

The boundary conditions in dimensionless form are:

$$x^+=0,\quad u^+=2\left(1-4r^{+2}\right),\ v^+=0,\ h^+=0$$
$$x^+>0,\quad r^+=0,\ \frac{\partial u^+}{\partial r^+}=0,\ v^+=0,\ \frac{\partial h^+}{\partial r^+}=0$$
$$r^+=0.5,\ u^+=0, v^+=0,\ \frac{\lambda^+}{c_p^+}\frac{\partial h^+}{\partial r^+}=1$$

The NIST Standard Reference Database 23 (REFPROP) Version 7 was used to calculate the temperature and pressure dependent properties of carbon dioxide. The calculated thermal properties were tabulated as functions of pressure and temperature with the thermal properties then obtained using second-order interpolations in the simulations.

Since the governing equations are parabolic in x, the solution can march in the downstream direction. The mesh used nonuniform control volumes to have more nodes near the wall. The governing equations were discretized utilizing the integral control volume method. In the solution, the algebraic forms of Eqs. (14) and (16) were first solved simultaneously for the unknowns u^+ and p^+ for a particular axial location. The radial velocities v^+ were then evaluated from the continuity equation, Eq. (13). Then the energy equation, Eq. (15), was integrated to calculate the enthalpies. The temperatures and thermophysical properties were then evaluated using second-order interpolation. The algorithm then recalculated u^+, p^+, v^+ and h^+ with the updated physical properties. Convergence was obtained when all of the following criterions were satisfied:

$$\left|\int_0^{1/2}\rho^+u^+r^+\,\mathrm{d}r^+-\frac{1}{8}\right|\leqslant 10^{-6}$$

$$\max\left|\frac{(u^+)_{i,j}^n-(u^+)_{i,j}^{n-1}}{(u^+)_{i,j}^n}\right|\leqslant 10^{-4}$$

$$\max\left|\frac{(v^+)_{i,j}^n-(v^+)_{i,j}^{n-1}}{\max((v^+)_{i,j}^{n-1})}\right|\leqslant 10^{-2}$$

$$\max\left|\frac{(h^+)_{i,j}^n-(h^+)_{i,j}^{n-1}}{(h^+)_{i,j}^n}\right|\leqslant 10^{-4}$$

$$\left|\frac{(Nu_{x,w})_i^n-(Nu_{x,w})_i^{n-1}}{(Nu_{x,w})_i^n}\right|\leqslant 5\times 10^{-3}$$

$$\left|\frac{\left(\frac{\mathrm{d}p^+}{\mathrm{d}x^+}\right)_i^n-\left(\frac{\mathrm{d}p^+}{\mathrm{d}x^+}\right)_i^{n-1}}{\left(\frac{\mathrm{d}p^+}{\mathrm{d}x^+}\right)_i^n}\right|\leqslant 5\times 10^{-3}$$

$$\left|\frac{\left(\frac{\mathrm{d}p^+}{\mathrm{d}x^+}\right)_i^*-\left(\frac{\mathrm{d}p^+}{\mathrm{d}x^+}\right)_i^n}{\left(\frac{\mathrm{d}p^+}{\mathrm{d}x^+}\right)_i^n}\right|\leqslant 10^{-2}$$

$$\left|\frac{(\overline{h^+})_i^*-(\overline{h^+})_i^n}{(\overline{h^+}_i^n)}\right|\leqslant 10^{-2},\quad \left|\frac{(q_w)_i^n-(q_w)_i^{n-1}}{(q_w)_i^n}\right|\leqslant 10^{-3}$$

Where the subscripts "i" and "j" are grid positions in the axial and radial directions; the superscript "n" represents the nth iteration; "$*$" represents the values obtained by the integration, and the overbar "-" indicates average values. After convergence at each location, the procedures were repeated for the next axial location. In the calculations, the x^+ direction had more than 2000 elements with 150 elements in the r^+ direction. The calculation stopped if flow reversal occurred. A more detailed description of the numerical methods used to solve the governing equations was given earlier [32].

The convective heat transfer parameters were then calculated from the converged results. For example, the local HTC on the inner wall was calculated according to Eq. (2). The pressure drop was calculated as:

$$p=\left|\rho_0u_0^2\sum_{j=2}^{N}\left(\left(\frac{\mathrm{d}p^+}{\mathrm{d}x^+}\right)_j(x^+)_j\right)\right| \tag{17}$$

The reliability of the numerical model was verified earlier [32,33]. For example, the numerical results for forced convective heat transfer of water with constant properties agreed very well with a separate computer program written to solve only the differential equations with constant properties in the same manner. For constant thermophysical properties, the problem can also be solved analytically [34]. The predicted Nu_x for constant properties agreed very well with the analytical results

in [34]. The Nusselt numbers for constant properties were correlated as [33]:

$$Nu_x^{cp} = \frac{q_w d}{(T_w(x) - T_{f,b}(x))\lambda_f} = \begin{cases} 1.030(\frac{1}{Pe}\frac{x}{d})^{-1/3} & (\text{when } \frac{1}{Pe}\frac{x}{d} \leqslant 0.01) \\ 2.221(\frac{1}{Pe}\frac{x}{d})^{-0.166} & (\text{when } 0.01 \leqslant \frac{1}{Pe}\frac{x}{d} \leqslant 0.055) \\ 3.656 & (\text{when } \frac{1}{Pe}\frac{x}{d} \geqslant 0.055) \end{cases} \quad (18)$$

The maximum deviations of Eq. (18) from the numerical results are ±3.0%, ±3.1%, and 1.0% for the three regions.

In addition, previous works [32,33] have shown that for small temperature differences between the wall and the fluid, the numerical results for the local HTC with variable thermophysical properties are very close to the values of the local HTC for constant thermophysical properties. The variable properties have little influence on the heat transfer for water but dramatically increase the diffusion mass transfer, with the buoyancy enhancing both the heat and mass transfer.

4. Results and discussion

4.1. Convection heat transfer of supercritical pressure CO_2 for upward flow

Figs. 4, 5, 8(a), 9 and 10 compare the numerical predictions with the experimental results for the local HTC. In these figures, the symbols are the experimental data and the lines are the numerical results. Bo^* is the buoyancy number, which was defined based on the properties at $x/d = 15$ [9]:

$$Bo^* = Gr^*/(Re^{3.425}Pr^{0.8}) \quad (19)$$

According to Jackson and Hall [9], for turbulent flow the buoyancy will significantly influence the heat transfer for $Bo^* > 5.6 \times 10^{-7}$.

Figs. 4 and 5 illustrate the local HTCs for different inlet fluid temperatures at an inlet pressure of 8.58 MPa and a lower heat flux of 4.69 kW/m^2 (Fig. 4) and an inlet pressure of 9.52 MPa and a higher heat flux of 13.0 kW/m^2 (Fig. 5). The inlet temperature strongly influences the convection heat transfer for a given pressure, mass flow rate and heat flux due to the strong variations of the thermophysical properties of supercritical CO_2 with temperature. The inlet pressure in Fig. 4 of 8.58 MPa is closer to the critical pressure of CO_2 ($p_{cr} = 7.38$ MPa) than the 9.52 MPa used in Fig. 5. Therefore, the influence of inlet temperature on the convection heat transfer in Fig. 4 is more evident than in Fig. 5. For the higher heat flux of 13.0 kW/m^2 in Fig. 5, the differences between the predicted and measured local HTC increase along the tube due to the strong influence of buoyancy and the sharp decrease of dynamic viscosity with temperature around the pseudocritical point along the tube, which strongly increases the local Reynolds number of the flow. As noted by Holman [35], the critical Reynolds number, Re_{cr}, for transition from laminar to turbulent flow decreases with increasing buoyancy. The values of Re_{cr} can be as low as 200–400 for combined free and forced convection. The differences between the numerical results for laminar flow with variable thermophysical properties and buoyancy and the experimental data shown in Figs. 4 and 5 may be caused by the early transition from laminar to turbulent flow due to the strong buoyancy effect and the sharp decrease of dynamic viscosity with temperature along the tube. For the lower heat flux (4.69 kW/m^2) in Fig. 4, the differences between the numerical results and the experimental data for $x/d = 9.5$–18.5 are less than in Fig. 5. The increase in the local heat transfer coefficient near the exit can be attributed to axial conduction in the wall (see Section 4.2).

Figs. 6(a) and 7(a) show the numerically calculated velocity distributions for upward flow at x/d 10 for the same conditions as in Figs. 4 and 5, inlet pressure of 8.58 MPa and heat flux of 4.69 kW/m^2 in Fig. 6(a) and inlet pressure of 9.52 MPa and heat flux of 13.0 kW/m^2 in Fig. 7(a). The velocities near the wall increase due to buoyancy, so the velocities at the tube centerline decrease so that the velocity distribution across the tube has an M-shape due to the variable properties and buoyancy. This phenomenon becomes more evident with increasing x/d

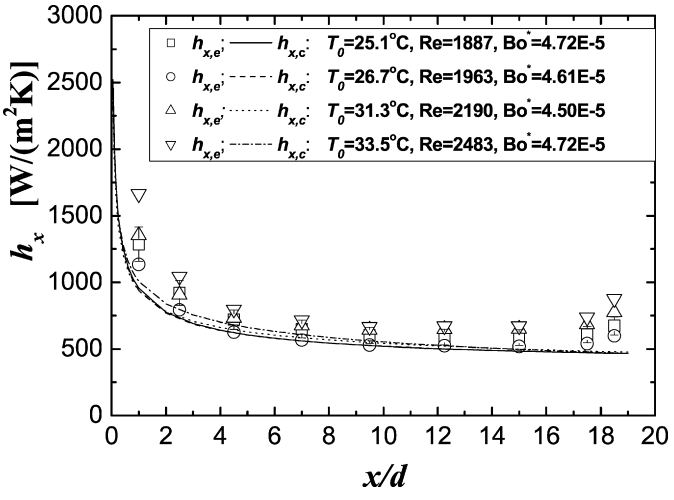

Fig. 4. Local heat transfer coefficients for various inlet temperatures for upward flow: $p_0 = 8.58$ MPa, $G = 6.29$ kg/(m^2 s), $q_w = 4.69$ kW/m^2.

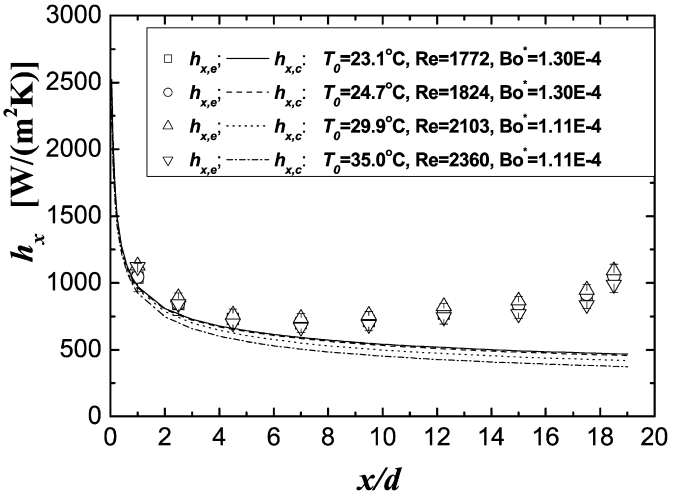

Fig. 5. Local heat transfer coefficients for various inlet temperatures for upward flow: $p_0 = 9.52$ MPa, $G = 6.34$ kg/(m^2 s), $q_w = 13.0$ kW/m^2.

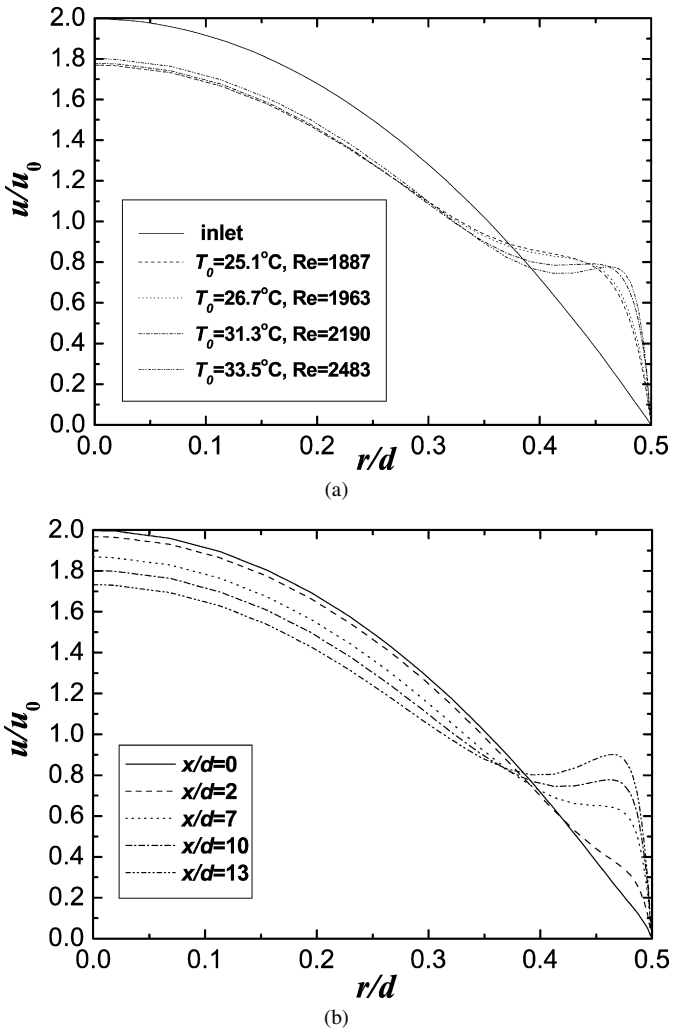

Fig. 6. Velocity distributions for upward flow (a) at $x/d = 10$ and (b) at various sections along the tube for $T_0 = 33.5$ °C and $Re = 2483$. $p_0 = 8.58$ MPa, $G = 6.29$ kg/(m^2 s), $q_w = 4.69$ kW/m^2.

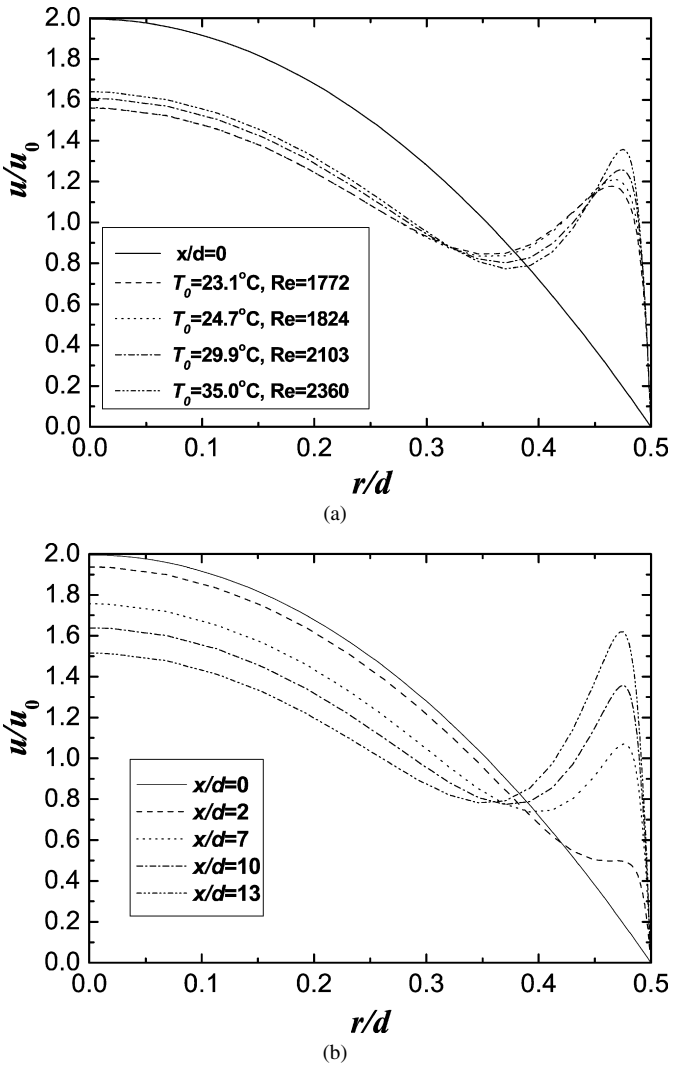

Fig. 7. Velocity distributions for upward flow (a) at $x/d = 10$ and (b) at various sections along the tube for $T_0 = 35.0°$ C and $Re = 2360$. $p_0 = 9.52$ MPa, $G = 6.34$ kg/(m^2 s), $q_w = 13.0$ kW/m^2.

and increasing heat flux as shown in Figs. 6(b) and 7(b). The deformation of the velocity distribution in the vertical tube may result in an early transition from laminar to turbulent flow and enhanced convection heat transfer (Figs. 4 and 5). The heat flux in Fig. 7 is 13.0 kW/m^2 which is higher than the heat flux in Fig. 6 of 4.69 kW/m^2; therefore, the deformation of the velocity distribution in the vertical tube is more evident in Fig. 7 than in Fig. 6.

Fig. 8 shows the local HTC and the numerically calculated velocity distributions at $x/d = 10$ for various heat fluxes at an inlet pressure of 9.57 MPa. For the lower heat flux (4.49 kW/m^2), the predicted HTC corresponds well with the experimental data (within 8%), which means that the flow is mainly laminar. For the higher heat fluxes (>13.7 kW/m^2), the HTC increases with increasing heat flux and then decreases with further increases in the heat flux. The differences between the measured and predicted HTCs increase along the tube (their difference is larger than 74% for $x/d = 15$), which are most likely due to the transition from laminar to turbulent flow under the strong influence of buoyancy and the sharp decrease of the dynamic viscosity with temperature around the pseudo-critical point along the tube, which strongly increases the local Reynolds number of the flow. The decreases of the HTC with further increases in the heat flux may be caused by laminarization which further reduces the convection heat transfer as shown previously [1–5,7–14,16,20–22,24,26–30]. The other possible reason may be the significant decrease of the density, thermal conductivity and specific heat when the temperature is much higher than the pseudocritical temperature. The velocity distributions in Fig. 8(b) further illustrate that the differences between the experimental data and the numerical results for the HTC are related to the strong deformation of the velocity profile and the influence of buoyancy.

Fig. 9 compares the measured and predicted local HTCs for various mass flow rates. The heat transfer is enhanced by the buoyancy, with the HTCs for smaller mass flow rates larger than those for larger mass flow rates due to the variation of the thermophysical properties and buoyancy. This is an interesting phenomenon that occurs with convection heat transfer of fluids at supercritical pressures.

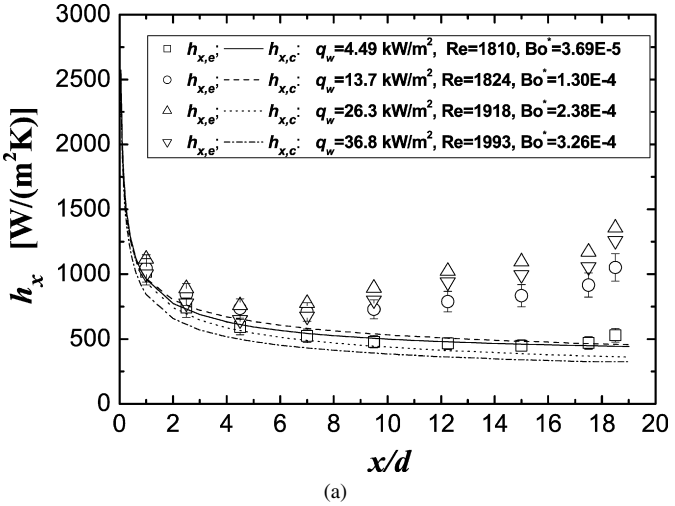

(a)

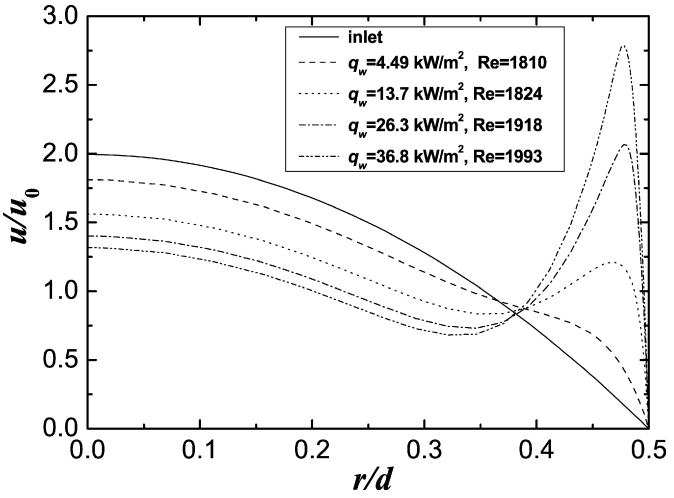

(b)

Fig. 8. (a) Local heat transfer coefficients for various heat fluxes and (b) velocity distributions at $x/d = 10$ for various conditions $p_0 = 9.57$ MPa, $G = 6.39$ kg/(m^2 s), $T_0 = 24.6\,^\circ$C.

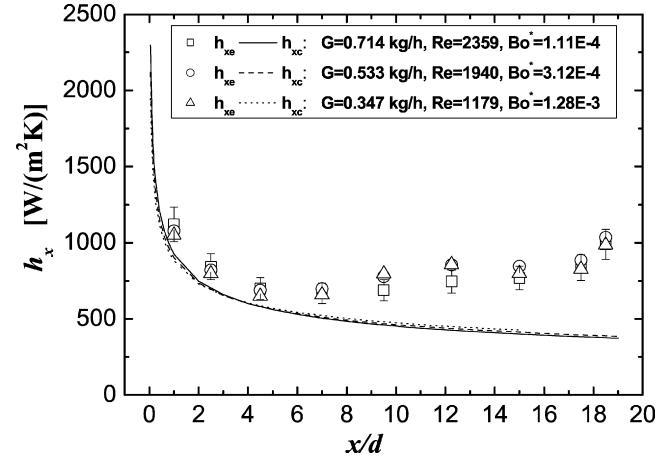

Fig. 9. Local heat transfer coefficients for various mass flow rates for upward flow $p_0 = 9.57$ MPa, $q_w = 12.3$ kW/m^2, $T_0 = 24.6\,^\circ$C.

Fig. 10 illustrates the influence of the inlet pressures on the local HTC. The local HTCs increase with decreasing pressure due to the sharp increase in c_p for pressures close to the critical pressure with the same mass flow rate, heat flux and inlet temperature. The numerical results corresponded well with the experimental data when buoyancy was not significant.

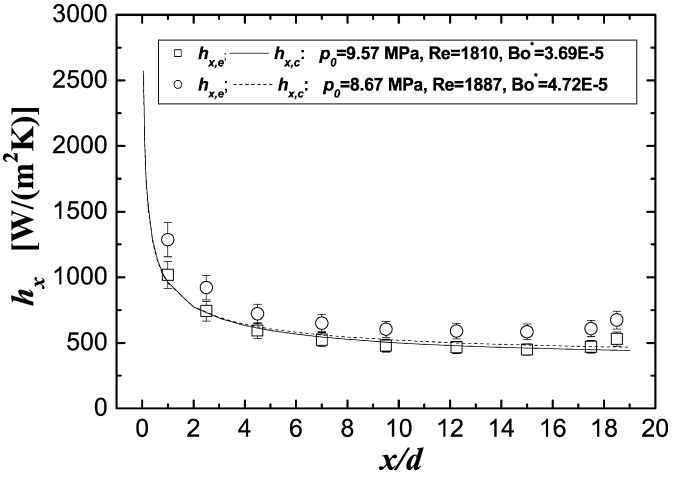

Fig. 10. Local heat transfer coefficients for various inlet pressures for upward flow $G = 6.48$ kg/(m^2 s), $q_w = 5.00$ kW/m^2, $T_0 = 24.7\,^\circ$C.

4.2. Wall effect on the convection heat transfer

In the experiments, some heat was also conducted along the axial direction in the tube wall. Analysis of the wall temperatures and the energy balance in the experimental and numerical studies showed that energy losses occur due to conduction along the wall near the test section inlet and outlet, which is referred to as the wall effect. To better simulate the convection heat transfer in the vertical tube, the numerical model was modified to include thermal conduction with an internal heat source in the wall together with the convection heat transfer in the vertical tube, with the calculational region including an unheated inlet section with length of $10d$, the test section with length of $20d$, and an unheated outlet section with length of $10d$.

The two-dimensional heat-conduction equation with an internal heat source used in the wall region is

$$\frac{\partial}{\partial x}\left(\lambda_s \frac{\partial T_s}{\partial x}\right) + \frac{1}{r}\frac{\partial}{\partial r}\left(r\lambda_s \frac{\partial T_s}{\partial r}\right) + q_v = 0 \tag{20}$$

The corresponding boundary conditions are:

$$x = 0, \quad \frac{\partial T_s}{\partial x} = 0; \qquad x = L_t, \quad \frac{\partial T_s}{\partial x} = 0$$

$$r = D/2, \quad q_w = -\lambda_s \frac{\partial T_s}{\partial x} = 0$$

$$r = d/2, T_{s,w} = T_{f,w} \text{ and } q_{s,w} = q_{f,w}$$

The calculation procedures were similar to the description in Section 3. In the calculations, the x^+ direction had more than 3200 elements (2000 elements in the test section, 600 elements in the unheated inlet section and 600 elements in the unheated outlet section) with 166 elements in the r^+ direction (150 elements in the flow region and 16 elements in the solid wall).

Fig. 11 compares the numerical results with and without the wall effect with the experimental data. The results show that the predictions with the wall effect more closely represent the

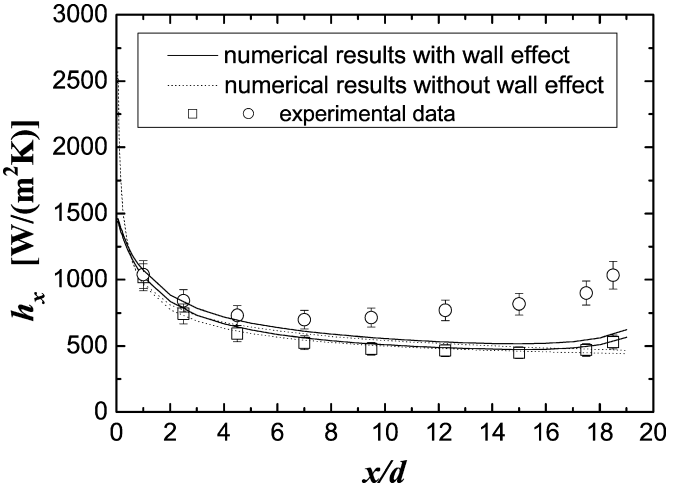

Fig. 11. Effect of wall conduction on the convection heat transfer for upward flow □: $p_0 = 9.57$ MPa, $G = 6.56$ kg/(m^2 s), $T_0 = 24.2\,^\circ$C, $q_w = 4.49$ kW/m^2, $Re = 1810$, $Bo^* = 3.69 \times 10^{-5}$. ○: $p_0 = 9.52$ MPa, $G = 6.30$ kg/(m^2 s), $T_0 = 23.1\,^\circ$C, $q_w = 13.8$ kW/m^2, $Re = 1772$, $Bo^* = 1.30 \times 10^{-4}$.

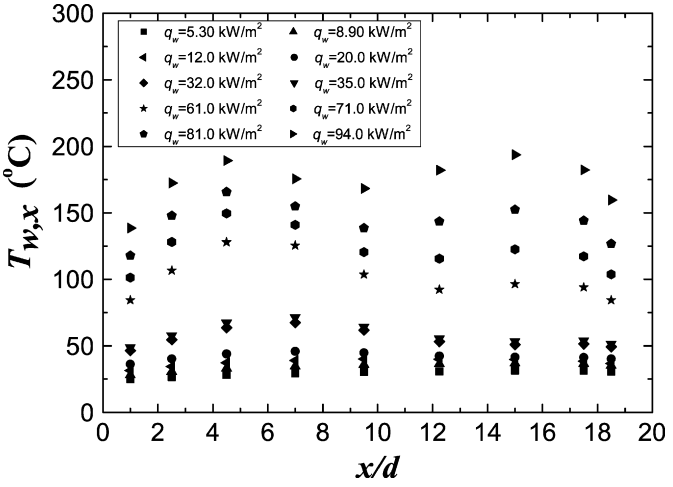

Fig. 12. Local wall temperatures for upward flow $p_0 = 8.85$ MPa, $G = 6.63$ kg/(m^2 s), $T_0 = 20.5\,^\circ$C, $Re = 1700$.

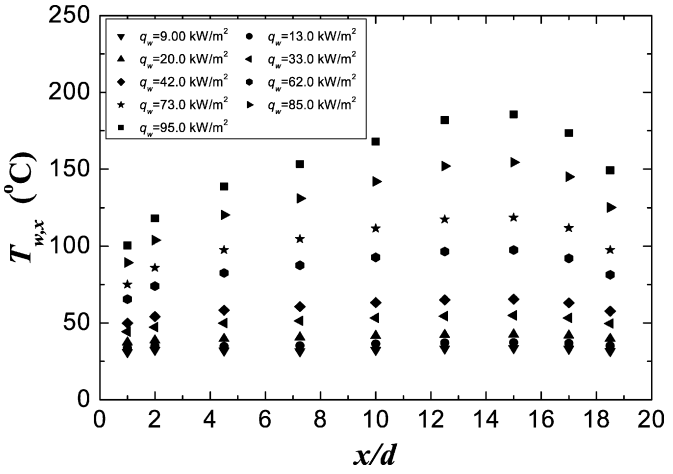

Fig. 13. Local wall temperatures for downward flow $p_0 = 8.85$ MPa, $G = 6.63$ kg/(m^2 s), $T_0 = 20.5\,^\circ$C, $Re = 1700$.

experimental data than those without the wall effect for the lower heat flux (4.49 kW/m^2). However, for the higher heat flux (13.8 kW/m^2), the numerical results with the wall effect are still much less than the experimental data, which means that the fluid flow has transitioned from laminar to turbulent flow due to the strong influence of buoyancy and the sharp decrease of dynamic viscosity with temperature along the tube.

4.3. Comparison of convection heat transfer for upward and downward flows

The effect of buoyancy on convection heat transfer in tubes is strongly influenced by the direction of the buoyancy force relative to the flow direction. The difference between the local heat transfer coefficients for upward and downward flows for the same experimental conditions reflect the effect of buoyancy on the convection heat transfer.

Fig. 12 shows the local wall temperature variations for upward flow (assisting flow) with $Re = 1700$. For a low heat flux (e.g., 5.30 kW/m^2), the local wall temperature increases continuously along the tube with a small decrease at the outlet due to the wall effect. For this case, the flow is laminar with little influence of buoyancy, as shown in Figs. 4, 6 and 10. For moderate heat fluxes (e.g., 8.90–35.0 kW/m^2), the local wall temperature first increases and then starts to decrease at $x/d = 7$, which is before the middle section of the tube (40% of the length from the inlet section) and far from the outlet section. This location is too far from the outlet to feel the wall effect. Therefore, this phenomenon may result from the transition from laminar to turbulent with the heat transfer enhanced by the strong buoyancy and the sharp decrease of dynamic viscosity with temperature along the tube, as shown in Figs. 5, 7, 8 and 11. For the higher heat fluxes (e.g., 61.0–94.0 kW/m^2), the local wall temperature first increases along the tube and then starts to decrease at $x/d = 4.3$, with the local wall temperature then increasing again at $x/d = 9.3$–12.2, with a small decrease at the outlet due to the wall effect. The first decrease of the local wall temperature at $x/d = 4.3$ is due to the transition from laminar to turbulent flow, while the local wall temperature increases along the tube at $x/d = 9.3$–12.2 may be caused by laminarization of the flow by the very strong buoyancy which reduces the convection heat transfer. The mechanism for this complex variation of the local wall temperature along the tube at very high heat fluxes needs further experimental and theoretical investigations.

Fig. 13 shows the local wall temperature variations for downward flow (opposing flow) with $Re = 1700$. For the moderate heat fluxes (e.g., 9.00 kW/m^2 and 13.0 kW/m^2), the local wall temperature first increases, then decreases at $x/d = 2$, with the local wall temperature almost constant after $x/d = 7.2$ with decreases at the outlet due to the wall effect. This phenomenon indicates that at the inlet the flow is laminar, with the buoyancy inducing very early transition from laminar to turbulent ($x/d \approx 2$), much earlier than for the upward flow (assisting flow) for the same conditions. For the high heat fluxes (e.g., 20.0–95.0 kW/m^2), the local wall temperature increases continuously along the tube with decreases at the outlet due to the wall effect, with the local temperatures much lower than for up-

ward flow with the same conditions, as shown in Figs. 12 and 13. These results indicate that with high heat fluxes, the flow in the tube is turbulent (due to the very strong buoyancy), and the heat transfer is more intensive than for upward flows with the same conditions. For all the conditions for downward flow, the convection heat transfer along the tube did not deteriorate as was observed for upward flow. This result is consistent with early investigations of mixed convection heat transfer in vertical tubes [1–5,7–14,16,20–22,24,26–30].

To further explore the flow transition from laminar to turbulent flow due to buoyancy, mixed convection heat transfer in a vertical tube and heat conduction in the tube wall were numerically simulated using FLUENT 6.1 [36]. The RNG k–ε turbulence model [37] and the Launder–Sharma turbulence model [38] were used in the numerical calculations for the turbulent flow. The SIMPLE algorithm [39] was used to couple the pressure and velocities. The second-order upwind advection model was used in the momentum, energy, turbulent kinetic energy, and turbulent energy dissipation equations. The convergence criteria required a decrease of at least 6 orders of magnitude for the residuals with no observable change in the outlet temperature for an additional 200 iterations. The computational domain was discretized into a rectangular mesh, typically with 520×85 (axial $\times$ radial) elements. The mesh was compressed in the radial direction towards the tube wall. The grid independence was investigated with grid distributions (axial $\times$ radial) of 320×85, 520×85 and 720×105 elements. The grid independence tests indicated that the grid having 520×85 elements ensured a satisfactory solution. This was verified by comparison of the computed wall temperatures for the 720×105 grid with those using the 520×85 grid with differences of less than 0.1 °C. The y^+ values at the first node of the mesh were always less than 1.0.

Fig. 14(a) compares the experimental results and the predictions. For the lower heat flux (e.g., 5.30 kW/m^2), buoyancy and the decrease of the dynamic viscosity with temperature along the tube are not significant and the flow remains laminar, so the predicted local wall temperatures with laminar flow are closer to the experimental data than the predicted results with the turbulence model. For the moderate heat flux (e.g., 8.90 kW/m^2), the buoyancy effect and the decrease of dynamic viscosity along the tube are more evident which results in transition from laminar to turbulent flow. In the first half of the tube, the predictions using the laminar model corresponded better to the measured local wall temperature, while in the second half of the tube the predictions with the turbulent flow model corresponded better to the measured data. These results reflect the transition from laminar to turbulent flow. For the higher heat flux (e.g., 35.0 kW/m^2), the buoyancy effect and the decrease of dynamic viscosity along the tube are more intense and the predicted wall temperatures using the RNG k–ε turbulence model and the Launder–Sharma turbulence model are closer to the experimental data in the later part of the tube, with the predictions using the Launder–Sharma turbulence model being somewhat better. These results further prove the occurrence of transition from laminar to turbulent flow due to the strong buoyancy and

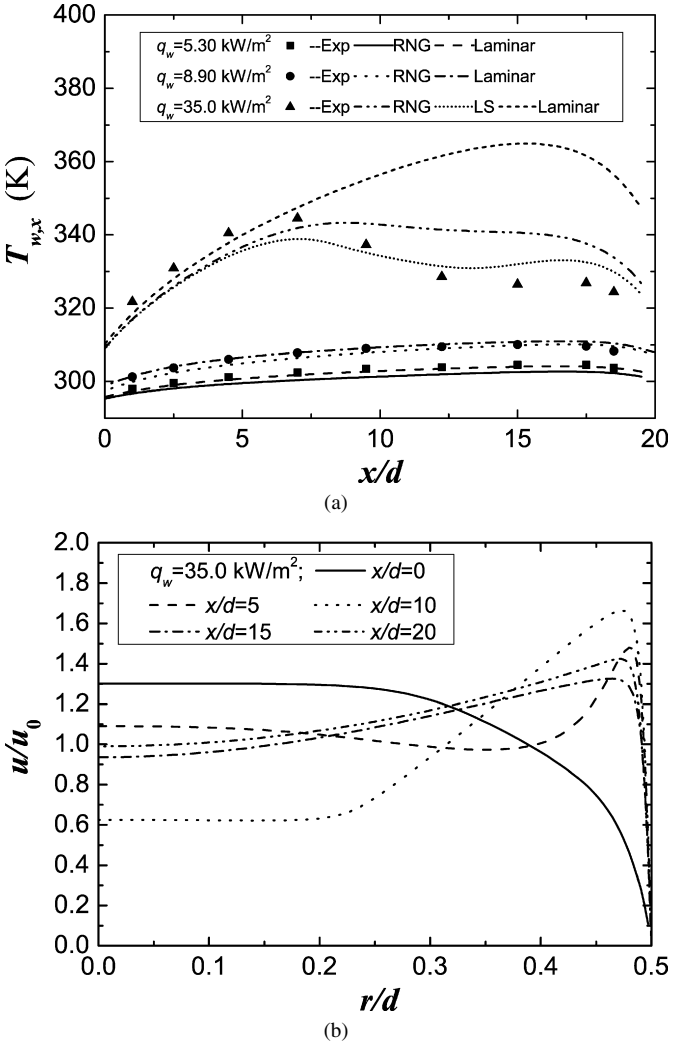

Fig. 14. (a) Local wall temperatures and (b) velocity distributions with $q_w = 3.5 \times 10^4$ W/m^2 for upward flow $p_0 = 8.85$ MPa, $T_0 = 20.5$ °C, $G = 6.63$ kg/(m^2 s), $Re = 1700$.

the sharp decrease of dynamic viscosity along the tube and verify the analysis of the results in Figs. 5, 8(a), 9, 11–13.

Fig. 14(b) shows the predicted velocity distributions for $q_w = 35.0$ kW/m^2 at various x/d. The velocity near the wall increases while the velocity near the center decreases so that the velocity distribution across the tube has an M-shape due to the variable properties and buoyancy. The velocity distribution deformation in the vertical tube then results in early transition from laminar to turbulent flow which enhances the convection heat transfer (Fig. 14(a)).

Fig. 15 shows the influence of flow direction and heat flux on the convection heat transfer when the inlet fluid temperature is much less than the pseudocritical temperature ($T_{pc} = 39$ °C for $p = 8.85$ MPa). The heat transfer coefficient increases with increasing heat flux and then decreases with further increases in the heat flux for both upward and downward flows. The increase in the heat transfer coefficient with increasing heat flux for the moderate heat fluxes is caused by the variation of the thermophysical properties, especially the sharp increase of c_p (see Fig. 1) and the influence of buoyancy and the decrease

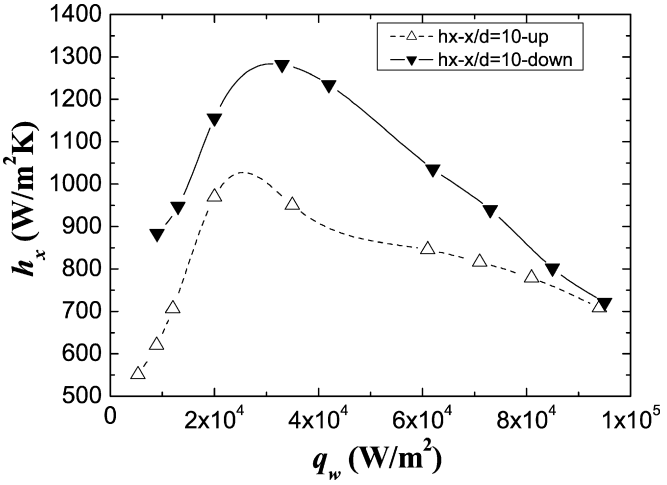

Fig. 15. Heat transfer coefficients for upward and downward flows with various heat fluxes $p_0 = 8.85$ MPa, $G = 6.63$ kg/(m^2 s), $T_0 = 20.5\,^\circ$C, $Re = 1700$, $x/d = 10$. Solid symbols: downward flow, hollow symbols: upward flow.

of dynamic viscosity along the tube which produces an early transition from laminar to turbulent flow for both upward and downward flows. The decrease in the convection heat transfer coefficient with further increases in the heat flux for the higher heat fluxes is caused by variations of the thermophysical properties (see Fig. 1) for downward flow. When the wall temperature is much higher than the pseudocritical temperature, most of the fluid in the tube is vapor, so the density, thermal conductivity and specific heat are reduced significantly. This reduces the convection heat transfer even for turbulent flow. However, for upward flow, the decrease in the convection heat transfer coefficient with increasing heat flux for the higher heat fluxes was caused not only by the variation of the thermophysical properties, but also by laminarization of the turbulence by the buoyancy. Fig. 15 shows that for very high heat fluxes (e.g., 90.0 kW/m^2), the convection heat transfer coefficients for both upward and downward flows are very similar because for very high heat fluxes the forced convection in the tube is negligible and the heat transfer is mainly controlled by the natural convection so the effect of the forced flow direction is not significant.

Fig. 16 illustrates the local heat transfer coefficient for both upward and downward flows. For the lower heat fluxes (e.g., 1.70–5.11 kW/m^2) as shown in Fig. 16(a), the influence of buoyancy on the convection heat transfer for upward flow is not evident, while for downward flows the buoyancy reduces the heat transfer in the inlet region and enhances the heat transfer further down the tube due to the transition from laminar to turbulent. Therefore, the local heat transfer coefficient for downward flow is higher than that for upward flow in the latter part of the tube as shown in Fig. 16(a). For the high heat fluxes (e.g., 13.7–36.8 kW/m^2) as shown in Fig. 16(b), the influence of buoyancy and decrease of dynamic viscosity along the tube on the convection heat transfer is significant for both upward and downward flows. For downward flow buoyancy enhances the heat transfer in the whole tube, while for upward flow buoyancy enhances the heat transfer only in the latter part of the tube. Generally, the difference between the local HTC for

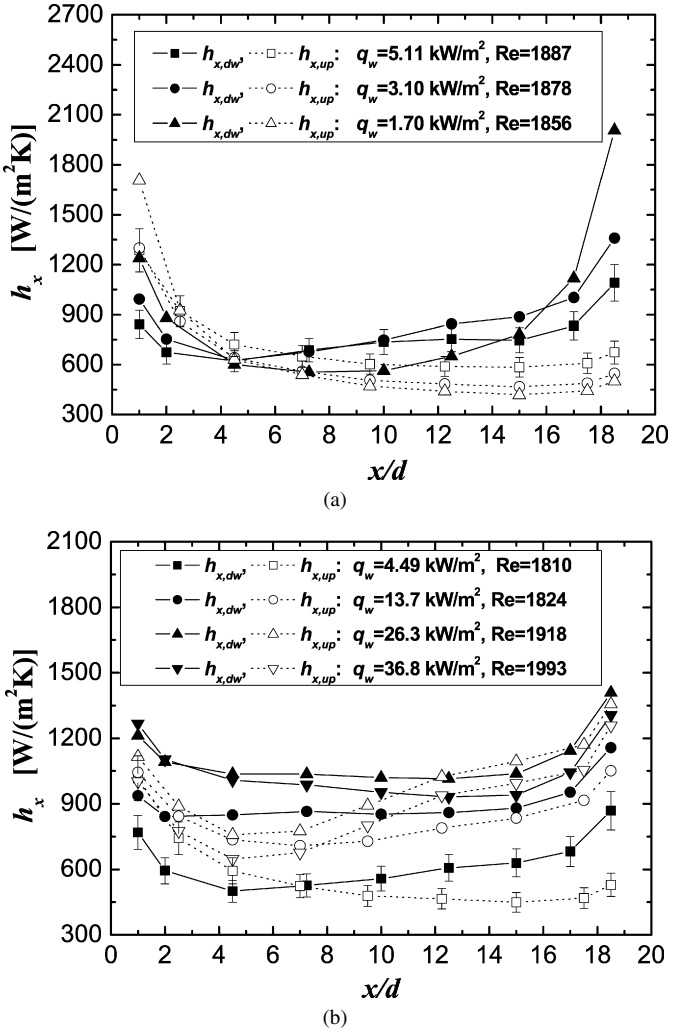

Fig. 16. Influence of flow direction on the local heat transfer coefficients (a) $p_0 = 8.66$ MPa, $G = 6.41$ kg/(m^2 s), $T_0 = 25.0\,^\circ$C (b) $p_0 = 9.62$ MPa, $G = 6.39$ kg/(m^2 s), $T_0 = 24.6\,^\circ$C. Solid symbols: downward flow, hollow symbols: upward flow.

downward and upward flows is not significant in the latter part of the tube when very strong buoyancy effects are present.

5. Conclusions

(1) With increasing heat flux the velocity distribution across the tube develops into an M-shape due to the property variations and buoyancy. This phenomenon becomes more evident with increasing x/d and heat flux.

(2) For upward flow (assisting flow) and moderate heat fluxes (e.g., 8.90–35.0 kW/m^2), the local wall temperature does not increase continuously but even decreases along the tube. This phenomenon may be due to the transition from laminar to turbulent flow, with the heat transfer enhanced by the strong buoyancy and the sharp decrease of dynamic viscosity with temperature along the tube. For higher heat fluxes (e.g., 61.0–94.0 kW/m^2), the local wall temperature first increases along the tube, then decreases, and then increases again, with a second small decrease at the outlet due to the conduction along the wall. The first decrease of

the local wall temperature is due to transition from laminar to turbulent flow. The local wall temperature then increases again along the tube due to laminarization of the flow by the very strong buoyancy which reduces the convection heat transfer.

(3) For downward flow (opposing flow) and high heat fluxes (e.g., 20.0–95.0 kW/m^2), the local wall temperature increases continuously along the tube with small decreases at the outlet due to conduction in the wall. The convection heat transfer did not deteriorate along the tube for opposing flow as was observed for assisting flow. The results indicate that for downward flow the buoyancy induces very early transition from laminar to turbulent flow (much earlier than for upward flow) which increases the heat transfer coefficient compared to that for upward flow with the same conditions.

(4) For the low heat fluxes (e.g., 5.30 kW/m^2), buoyancy and the decrease of dynamic viscosity with temperature along the tube are not significant and the flow remains laminar, so the predictions with the laminar flow model for the local wall temperatures are closer to the experimental data than those with the turbulent model. In addition, the numerical results with the wall effect more closely represent the experimental data than those without wall effect. For the moderate heat fluxes (e.g., 8.90 kW/m^2), the buoyancy effect and the decrease of dynamic viscosity along the tube are more evident which results in transition from laminar to turbulent flow. For the high heat fluxes (e.g., 35.0 kW/m^2), the buoyancy effect and the decrease of dynamic viscosity along the tube are more intense so the predicted wall temperatures using the RNG k–ε turbulence model and the Launder–Sharma turbulence model agree much better with the experimental data than the laminar flow predictions for most of the tube, with the Launder–Sharma turbulence model giving the best results.

(5) For $T_{f0} < T_{pc}$, the HTC increases with increasing heat flux and then decreases with further increases in the heat flux for both upward and downward flows. For downward flow the decreases of the HTC with increasing heat flux for the higher heat fluxes were caused by variations of the thermophysical properties (sharp decreases of c_p, λ, ρ). However, for upward flows, the decreases of the HTC with increasing heat flux for the higher heat fluxes were caused not only by the variations of the thermophysical properties, but also by laminarization of the turbulence by the buoyancy. Therefore, the HTCs for upward flow are less than for downward flow. For very high heat fluxes (e.g., 90.0 kW/m^2), the HTCs for both upward and downward flows were very similar because the heat transfer is mainly controlled by the natural convection.

(6) For downward flow the buoyancy enhanced the heat transfer coefficients along the entire tube, while for upward flow the buoyancy enhanced the heat transfer coefficients only in the latter part of the tube. Generally, the difference between the local heat transfer coefficients for downward and upward flows was not evident in the latter part of the tube when very strong buoyancy effects were present.

Acknowledgements

This project was supported by the National Outstanding Youth Fund from the National Natural Science Foundation of China (No. 50025617). We thank Professor J.D. Jackson in the School of Mechanical, Aerospace and Civil Engineering, the University of Manchester, UK, for many discussions and good suggestions for the research. We also thank Prof. David Christopher for editing the English.

References

[1] B.S. Petukhov, Heat transfer in a single phase medium under supercritical conditions (survey), High Temperatures 6 (4) (1968) 696–709.

[2] B.S. Petukhov, Heat transfer and friction in turbulent pipe flow with variable physical properties, in: Advances in Heat Transfer, vol. 6, 1970, pp. 503–564.

[3] W.B. Hall, Heat transfer near the critical point, in: Advances in Heat Transfer, vol. 7, 1971, pp. 1–86.

[4] W.B. Hall, J.D. Jackson, Heat transfer near the critical point, Keynote Lecture, in: Proceedings of the 6th International Heat Transfer Conference, vol. 6, Toronto, Ontario, Canada, August 7–11, 1978, pp. 377–392.

[5] M.E. Shitsman, Impairment of the heat transmission at supercritical pressures, High Temperatures 1 (2) (1963) 237–244.

[6] E.A. Krasnoshchekov, V.S. Protopopov, Experimental study of heat exchange in carbon dioxide in the supercritical range at high temperature drops, High Temperatures 4 (3) (1966) 375–382.

[7] K. Yamagata, K. Nishikawa, S. Hasegawa, et al., Forced convective heat transfer to supercritical water flowing in tubes, Int. J. Heat Mass Transfer 15 (1972) 2575–2593.

[8] V.S. Protopopov, Generalizing relations for the local heat-transfer coefficients in turbulent flows of water and carbon dioxide at supercritical pressure in a uniformly heated circular tube, High Temperatures 15 (4) (1977) 687–692.

[9] J.D. Jackson, W.B. Hall, Influences of buoyancy on heat transfer to fluids flowing in vertical tubes under turbulent conditions, in: S. Kakac, D.B. Spalding (Eds.), Turbulent Forced Convection in Channels and Bundles, vol. 2, Hemisphere Publishing Corp., New York, USA, 1979, pp. 613–640.

[10] V.N. Popov, E.P. Valueva, Numerical modeling of mixed turbulent convection of helium at supercritical parameters of state in a vertical tube, Thermal Engrg. 35 (7) (1988) 399–404.

[11] A.F. Polyakov, Heat transfer under supercritical pressures, in: Advances in Heat Transfer, vol. 21, Academic Press, New York, 1991, pp. 1–53.

[12] V.A. Kurganov, A.G. Kaptilnyi, Flow structure and turbulent transport of a supercritical pressure fluid in a vertical heated tube under the conditions of mixed convection, Experimental data, Int. J. Heat Mass Transfer 36 (13) (1993) 3383–3392.

[13] V.A. Kurganov, Heat transfer and pressure drop in tubes under supercritical pressure of the coolant. Part 1: Specifics of the thermophysical properties, hydrodynamics, and heat transfer of the liquid. Regimes of normal heat transfer, Thermal Engrg. 45 (3) (1998) 177–185.

[14] V.A. Kurganov, Heat transfer and pressure drop in tubes under supercritical pressure of the coolant. Part 2: Heat transfer and friction at high heat fluxes. The Influence of additional factors. Enhancement of deteriorated heat transfer, Thermal Engineering 45 (4) (1998) 301–310.

[15] J. Pettersen, A. Hafner, G. Skaugen, et al., Development of compact heat exchangers for CO_2 air-conditioning systems, Int. J. Refrigeration 21 (3) (1998) 180–193.

[16] J.D. Jackson, Some striking features of heat transfer with fluids at pressures and temperatures near the critical point, Keynote Paper for International Conference on Energy Conversion and Application (ICECA '2001), Wuhan, China.

[17] S.S. Pitla, E.A. Groll, S. Ramadhyani, New correlation to predict the heat transfer coefficient during in-tube cooling of turbulent supercritical CO_2, Int. J. Refrigeration 25 (7) (2002) 887–895.

[18] S.M. Liao, T.S. Zhao, An experimental investigation of convection heat transfer to supercritical carbon dioxide in miniature tubes, Int. J. Heat Mass Transfer 45 (2002) 5025–5034.
[19] S.H. Yoon, J.H. Kim, Y.W. Hwang, et al., Heat transfer and pressure drop characteristics during the in-tube cooling process of carbon dioxide in the supercritical region, Int. J. Refrigeration 26 (2003) 857–864.
[20] P.X. Jiang, Y.J. Xu, J. Lv, et al., Experimental investigation of convection heat transfer of CO_2 at supercritical pressures in vertical mini tubes and in porous media, Appl. Thermal Engrg. 24 (2004) 1255–1270.
[21] S. He, W.S. Kim, P.X. Jiang, et al., Simulation of mixed convection heat transfer to carbon dioxide at supercritical pressures, Int. J. Mech. Engrg. Sci. Part C 218 (2004) 1281–1296.
[22] I.L. Pioro, H.F. Khartabil1, R.B. Duffey, Heat transfer to supercritical fluids flowing in channels—empirical correlations (survey), Nuclear Engrg. Design 230 (2004) 69–91.
[23] S. He, P.X. Jiang, Y.J. Xu, et al., A computational study of convection heat transfer to CO_2 at supercritical pressures in a vertical mini tube, Int. J. Thermal Sci. 44 (2005) 521–530.
[24] M. Bazargan, D. Fraser, V. Chatoorgan, Effect of buoyancy on heat transfer in supercritical water flow in a horizontal round tube, J. Heat Transfer 127 (2005) 897–902.
[25] M.H. Anderson, J.R. Licht, M.L. Corradini, Progress on the University of Wisconsin supercritical water heat transfer facility, in: The 11th International Topical Meeting on Nuclear Reactor Thermal-Hydraulics (NURETH-11), Paper: 265, Popes' Palace Conference Center, Avignon, France, October 2–6, 2005.
[26] P. Asinari, Numerical prediction of turbulent convective heat transfer in mini/micro channels for carbon dioxide at supercritical pressure, Int. J. Heat Mass Transfer 48 (18) (2005) 3864–3879.
[27] R.B. Duffey, I.L. Pioro, Experimental heat transfer of supercritical carbon dioxide flowing inside channels (survey), Nuclear Engrg. Design 235 (2005) 913–924.
[28] I.L. Pioro, R.B. Duffey, Experimental heat transfer in supercritical water flowing inside channels (survey), Nuclear Engrg. Design 235 (2005) 2407–2430.
[29] M. Van der Kraan, M.M.W. Peeters, M.V. Fernandez Cid, et al., The influence of variable physical properties and buoyancy on heat exchanger design for near- and supercritical conditions, J. Supercritical Fluids 34 (2005) 99–105.
[30] J.H. Bae, J.Y. Yoo, H. Choi, Direct numerical simulation of turbulent supercritical flows with heat transfer, Phys. Fluids 17 (2005) 105104.
[31] P.X. Jiang, R.F. Shi, Y.J. Xu, et al., Experimental investigation of convection heat transfer of CO_2 at supercritical pressures in a porous tube, J. Supercritical Fluids 38 (2006) 339–346.
[32] P.X. Jiang, Convective heat and mass transfer of water at sub- or supercritical pressures, Post Doctoral Research Report, Tsinghua University, Beijing, 1993 (in Chinese).
[33] P.X. Jiang, Z.P. Ren, B.X. Wang, Forced and mixed convective diffusion of iron corrosion products in water in vertical tubes, in: 29th National Heat Transfer Conference, Atlanta, USA, 1993, pp. 365–370.
[34] B.S. Petukhov, L.G. Genin, S.A. Kovalev, Heat Transfer in Nuclear Power Equipment, Energoatomizdat Press, Moscow, 1986 (in Russian).
[35] J.P. Holman, Heat Transfer, eighth ed., McGraw–Hill, 1997, pp. 372–377.
[36] FLUENT User's Guide, Release 6.1. FLUENT Inc., Lebanon, 2001.
[37] V. Yakhot, S.A. Orszag, Renormalization group analysis of turbulence: I. Basic theory, J. Sci. Computing 1 (1) (1986) 1–51.
[38] B.E. Launder, B.I. Sharma, Application of the energy-dissipation model of turbulence to the calculations of flow near a spinning disc, Lett. Heat Mass Transfer 1 (1974) 131–138.
[39] S.V. Patankar, D.B. Spalding, A calculation procedure for heat, mass and momentum transfer in three-dimensional parabolic flows, Int. J. Heat Mass Transfer 15 (1972) 1787–1806.